

# Atomistic Simulations on the Tensile Deformation Behaviors of Three-Dimensional Graphene

Yang Liu, Jianjun Liu, Shaofeng Yue, Junqing Zhao, Bin Ouyang, and Yuhang Jing\*

Molecular dynamics simulations is used to investigate the mechanical properties of three-dimensional (3D) graphene under uniaxial tensile loading. The results show that the tensile deformation of 3D graphene exhibits size dependence along both armchair and zigzag directions. By analyzing the atomic von Mises stress and structural evolution, compared to the 3D graphene with smaller in-plane cell size, the larger 3D graphene exhibits two typical deformation events, i.e., transverse structural shrinkage and axial elastic deformation. The fracture stress of 3D graphene is much smaller than that of 2D graphene because of its porous structure. However, the fracture strain of 3D graphene is larger than that of 2D graphene due to the larger transverse structural shrinkage along both armchair and zigzag directions. Effects of temperature, strain rate, and thickness of 3D graphene on the tensile behavior is investigated. The simulation results indicate that the fracture stress and the fracture strain decrease with increasing temperature and with decreasing strain rate. However, the fracture stress and the fracture strain is not dependent on the thickness of 3D graphene. The results in this paper suggest that 3D graphene with higher stretchability tunable by in-plane cell size can be promising multifunctional materials for many engineering applications.

## 1. Introduction

Graphene, a two-dimensional monolayer of graphite, has attracted tremendous interests<sup>[1–5]</sup> because of its superior physical properties, such as large carrier mobility,<sup>[1]</sup> extremely high thermal conductivity<sup>[2]</sup> and exceptional mechanical

strength.<sup>[3]</sup> The discovery of new multi-functional carbon allotrope has been the focus of experimental and theoretical explorations due to its fundamental scientific and technological significance. Recently fabricated carbon Ene-yne graphyne<sup>[6]</sup> presents much higher stretchability compared to pristine graphene, which has potential applications in stretchable and flexible nanodevices.<sup>[7]</sup> However, for larger-scale potential applications, three-dimensional (3D) graphene networks are needed by assembly of two-dimensional (2D) graphene sheets.<sup>[8–11]</sup> Compared with 2D graphene sheets, the 3D graphene architectures not only possess a bulk form which is compatible with conventional electronic technology, but provide porous structures which can make them very promising in energy and environmental applications. Recently, 3D graphene has been synthesized experimentally<sup>[12]</sup> about two decades after theoretical prediction.<sup>[13]</sup> The 3D graphene retains the strong covalent bonding. The structures of 3D graphene hold very high stabilities.<sup>[12]</sup> A representative structure of 3D graphene is


shown in **Figure 1**. Three graphene sheets are joined together through  $sp^2$  bonding. Recent density functional theory (DFT) calculations<sup>[14]</sup> verify the geometric structures of 3D graphene and superb mechanical and thermal properties are found for the 3D graphene. In the meanwhile, the unique electronic structure of 3D graphene is reported and its thermoelectric figure of merit (ZT) is an order of magnitude larger than that of graphene.<sup>[15]</sup> 3D thin polymer films sandwiched between two 2D graphene layers exhibit anisotropic thermal characteristics.<sup>[16,17]</sup> Materials with different mechanical, thermal, and electrical properties are needed to design smart and functional devices. However, little theoretical work on the mechanical properties of 3D graphene, particularly the deformation and failure mechanism, have been reported.<sup>[14,18–20]</sup> Recently, high specific strength and anomalous Poisson ratio in 3D graphene are found based on DFT calculations.<sup>[14]</sup> The high specific strength and anisotropic Poisson ratio may be utilized to design multifunctional structures used for biomedical engineering or energy systems.<sup>[21,22]</sup> The in-plane compression and out-of plane nano-indentation simulations on the 3D graphene display that the Young's modulus of the 3D graphene is dominated by the hinge density and a highly localized compression behavior is observed.<sup>[18]</sup> Very recently, out-of-plane compressive

Dr. Y. Liu, Dr. J. Liu  
Jiangsu Electric Power Company Research Institute, Nanjing 211103, P.R. China

Dr. Yue, J. Zhao, Dr. Y. Jing  
Department of Astronautical Science and Mechanics  
Harbin Institute of Technology, Harbin 150001, P.R. China  
E-mail: jingyh@hit.edu.cn

Dr. Ouyang, Dr. Y. Jing  
National Center for Supercomputing Applications  
University of Illinois at Urbana-Champaign, Urbana, IL 61801, USA

Dr. Y. Jing  
Beckman Institute for Advanced Science and Technology  
University of Illinois at Urbana-Champaign, Urbana, IL 61801, USA

 The ORCID identification number(s) for the author(s) of this article can be found under <https://doi.org/10.1002/pssb.201700680>.

DOI: 10.1002/pssb.201700680

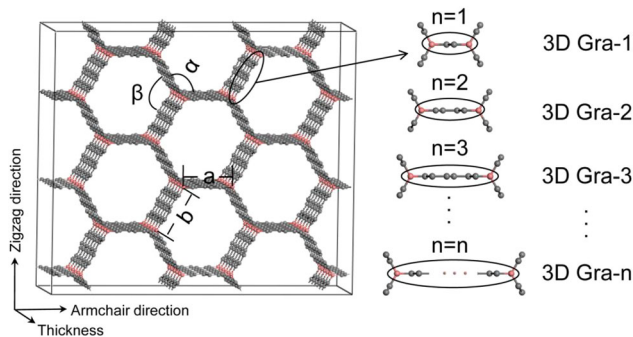


**Figure 1.** Schematic of 3D Gra-*n* structure with the definition of *n*. Armchair, zigzag, and thickness directions are denoted by arrows.

deformation behaviors of 3D graphene are investigated by combining atomistic simulations and continuum modeling.<sup>[19]</sup> Two critical deformation events, elastic mechanical instability and inelastic structural collapse, are revealed. However, to our knowledge, investigation on the tensile behaviors of 3D graphene in the literature is limited.<sup>[20]</sup>

In this work, we employ classical molecular dynamics (MD) to investigate the mechanical properties and the fracture process of 3D graphene under uniaxial tensile loading. The elastic properties and tensile behavior such as fracture stress and fracture strain are studied. Additionally, temperature, strain rate, and size effects on the fracture process are explicitly considered.

## 2. Model Structure and Simulation Methodology

The structures of 3D graphene are constructed for this work, as shown in Figure 1. Every three graphene sheets are linked together through  $sp^2$  bonding at an angle  $120^\circ$  between two sheets. We define “*n*” in 3D Gra-*n* as a 3D graphene structure in which there are *n*-zigzag lines between the nearest-neighboring junctions. For simplicity, only the ordered 3D graphene structures are considered in the current work, where the in-plane cell sizes, *a* and *b*, are equal.

We perform a series of MD simulations to investigate the tensile behavior of 3D Gra-*n* structures in both armchair and zigzag direction. The interaction between carbon atoms of the 3D graphene is described by the adaptive intermolecular reactive empirical bond order (AIREBO) potential with van der Waals interaction, which derived from the second-generation Brenner potential.<sup>[23,24]</sup> The AIREBO potential is extensively used in MD simulation of graphene and can accurately compute the bond–bond interaction, bond breaking, and bond reforming in the carbon atoms. The optimized parameters we adopted in this paper are also usually used for computing the mechanical properties of other carbon-based materials, such as graphene,<sup>[25]</sup> carbon nanotubes,<sup>[26]</sup> and graphene nanoribbons.<sup>[27]</sup>

The LAMMPS package<sup>[28]</sup> is used to perform all MD simulations in our study. The Velocity–Verlet algorithm is used to integrate the equations of motion with a time step of 0.1 fs. All systems are equilibrated at a constant pressure of 1 atm and a given temperature using NPT (constant atom number, pressure, and temperature) for 200 ps. The temperature is controlled by employing the Nosé–Hoover thermostat.<sup>[29]</sup> After the NPT relaxation, the engineering strain is then applied along the uniaxial direction to perform uniaxial tensile tests. The strain increment is applied to the structure every 10 000 to 500 time steps. The stress is calculated every last 5000–250 time steps in the form,

$$\sigma = \frac{1}{V} \sum_i [-m_i v_i \otimes v_i + \frac{1}{2} \sum_{j \neq i} r_{ij} \otimes f_{ij}],$$

where  $m_i$  and  $v_i$  are the mass and velocity of atom *i*,  $f_{ij}$  are the forces between atoms *i* and *j*,  $r_{ij}$  are the projection of the inter-atomic distance vectors along the tensile direction, and *V* is the total volume. The corresponding strain rates vary from 0.001 ps<sup>−1</sup> to 0.02 ps<sup>−1</sup>. Periodic boundary conditions are applied along the armchair and zigzag directions to eliminate influence of the edge, and the free boundary condition is applied in the thickness direction.

## 3. Results and Discussion

Figure 2 show the stress–strain curves for 3D Gra-*n* under tensile loading along the armchair and zigzag directions,

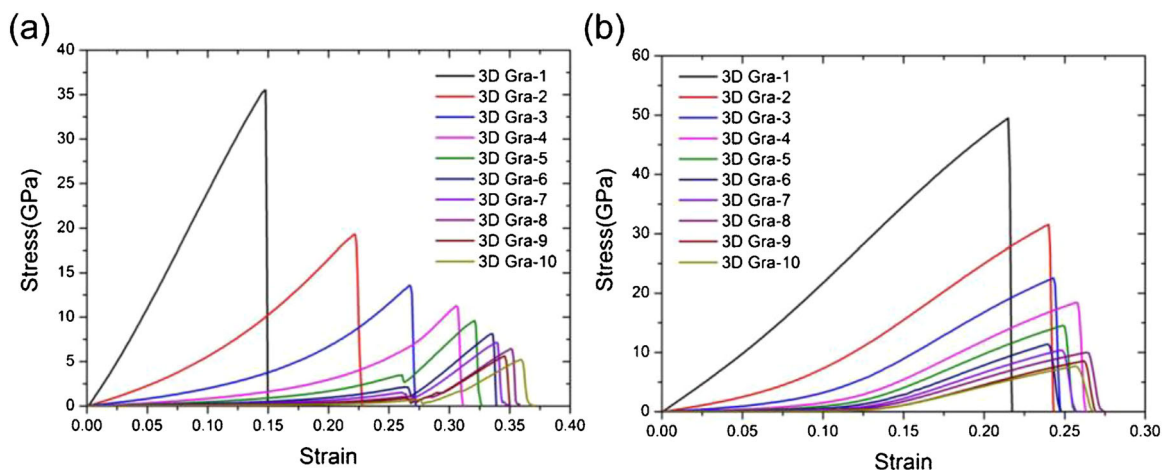


**Figure 2.** a) Stress–strain curves of 3D graphene under tensile loading along the armchair and b) zigzag directions simulated at 300 K with strain rate of 0.001 ps<sup>−1</sup>.

respectively, simulated at 300 K, with strain rate of 0.001 ps<sup>-1</sup>. The corresponding in-plane cell size of the 3D graphene varies from 0.36 to 2.25 nm with the increase of  $n$  in 3D Gra- $n$  from 1 to 10. The thicknesses of all 3D Gra- $n$  structures are about 1.2 nm. The number of atoms varies from 9600 to 23436. The thickness dependence of mechanical properties will be investigated in detail later. From Figure 2, we can notice that the stress-strain curve is dependent on the in-plane cell size. For comparison, we also obtain the stress-strain curve of 2D graphene under tension along the zigzag and armchair directions (not shown for brevity). The calculated fracture stress of 2D graphene is 104.8 and 130.1 GPa along the armchair and zigzag directions, respectively, which are consistent with the previous theoretical results.<sup>[27,30]</sup> The fracture strain of 2D graphene is 0.14 and 0.21 along the armchair and zigzag directions, respectively, which are also consistent with the previous simulation results.<sup>[27]</sup> When the in-plane cell size is smaller ( $n = 1$ ), the tensile stress-strain curves of 3D graphene along the zigzag and armchair directions are similar to those of 2D graphene. The stress linearly increases with the increase of strain before fracture. However, the whole tensile stress-strain curves show strong nonlinearity when the in-plane cell size is increased ( $>1$  nm). There are two clear stages during the tensile process. These results indicate that the tensile deformation mechanisms of 3D graphene are quite different for different in-plane cell sizes, which will be revealed later.

The dependences of the fracture stress and strain of 3D graphene along the armchair and zigzag directions on the in-plane cell size are shown in Figure 3. It can be seen from Figure 3a that the fracture stress along both armchair and zigzag directions decreases monotonically with the increase of in-plane cell size, and vary slightly for the larger size. The fracture stress of 3D graphene is much smaller than that of 2D graphene because of the porous structures. Specifically, when the in-plane cell size is 0.36 nm, the fracture stress along the armchair and zigzag direction is 35.5 and 49.5 GPa, respectively. When the in-plane cell size is increased to 2.25 nm, the corresponding fracture stress along the armchair and zigzag direction is only 5.2 and 7.6 GPa, respectively. This trend is ascribed to the different atom densities of the 3D graphene caused by the cell size. With

the in-plane cell size of 3D graphene increasing from 0.36 to 2.25 nm, the corresponding atom density drops from 98.3 to 18.8 atom nm<sup>-3</sup>, which are much smaller than that of graphene (117.7 atom nm<sup>-3</sup>). The sparser carbon atoms in the 3D graphene lead to less bonding and consequently result in a smaller fracture stress. Different from the fracture stress, the fracture strain of 3D graphene has an opposite trend with respect to the in-plane cell size as shown in Figure 3b. It can be seen that as the size increases, the fracture strain of 3D graphene along both the armchair and zigzag directions increases. In comparison with the fracture strain along the zigzag direction, the fracture strain along armchair direction displays much larger change. When the in-plane cell size of 3D graphene is larger than 1 nm, the fracture strain of 3D graphene along the armchair direction is larger than 0.32, which shows better stretchability in comparison with 2D graphene (0.2)<sup>[27]</sup> and Ene-yne graphyne (0.3).<sup>[7]</sup> Nevertheless, the fracture stress is smaller than that of 2D graphene<sup>[27]</sup> and Ene-yne graphyne.<sup>[7]</sup>

In order to understand detailed underlying mechanism of in-plane cell size effects, two typical 3D graphenes (3D Gra-1 and -9) are further investigated. The stress-strain curves from Figure 2 are shown in Figure 4 again. The corresponding atomic configurational evolutions of 3D Gra-1 and -9 are studied. Figures 5 and 6 show a series of snapshots of these two 3D graphene during the tensile deformation along the armchair and zigzag directions. The variations of the graphene wall length and angle between two graphene walls in 3D Gra-1 and -9 (see Figure 1) with the strain during the tensile deformation along the armchair and zigzag directions are shown in Figure 7 in order to compare the mechanical responses of 3D graphene with 2D graphene.<sup>[27]</sup> For smaller size, as shown in Figure 4, the stress is linearly increased with the increase of strain along both armchair and zigzag directions. The fracture strain along the zigzag direction is larger than that along the armchair direction. Similar to previous reports on the 2D material with hexagon structures,<sup>[27,31]</sup> this phenomenon is mainly attributed to the different elongation ratio of graphene wall and angle variation between two graphene walls as shown in Figure 7 when 3D graphene is under tensile loading along the armchair and zigzag

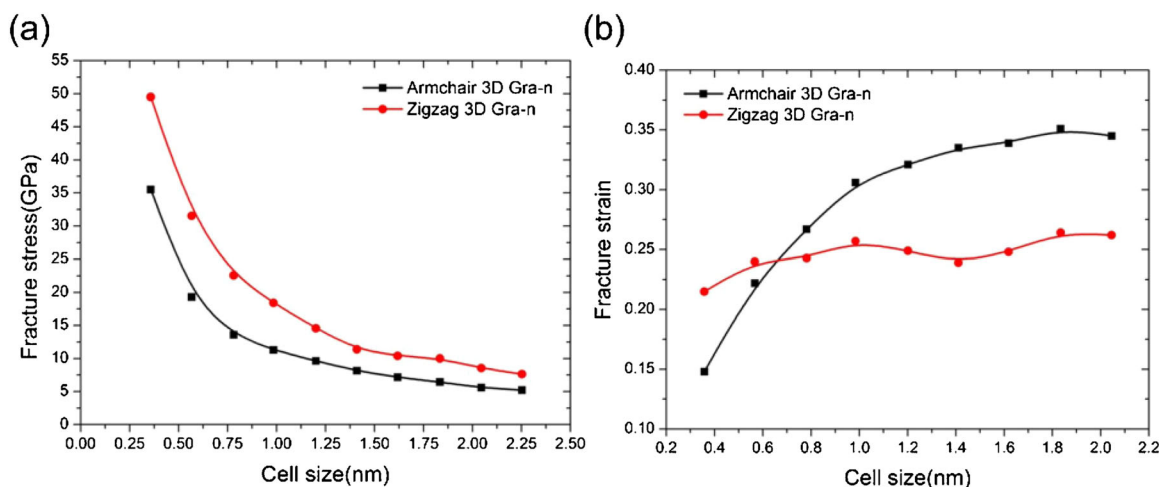


**Figure 3.** a) The variations of fracture stress and b) fracture strain with the in-plane cell size of 3D graphene along the armchair and zigzag directions at 300 K with strain rate of 0.001 ps<sup>-1</sup>.



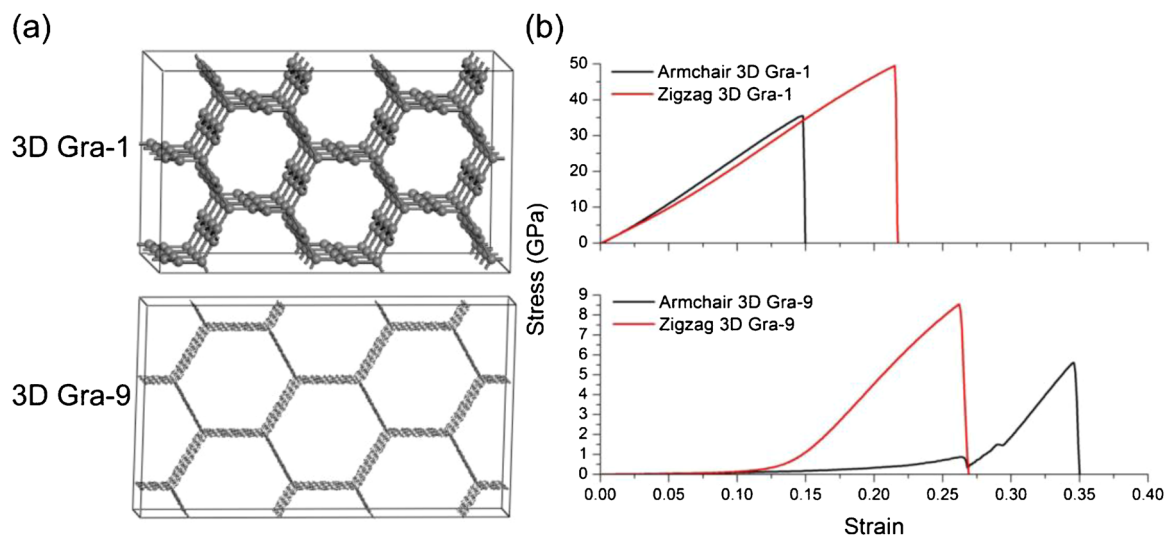


**Figure 4.** a) 3D Gra-1 and -9 structures. b) Stress–strain curves for 3D Gra-1 and -9 along the armchair and zigzag directions at 300 K with strain rate of 0.001 ps<sup>-1</sup>.

directions. From **Figure 5**, it can be seen that the stress of junction are gradually enlarged during the tensile process for both armchair and zigzag directions and reach a maximum. The stress mainly concentrates near junctions, which lead to a brittle fracture.

While for the stress-strain curve of 3D Gra-9, there are two stages: transverse structural shrinkage and axial elastic deformation. For

the tension along zigzag direction, in the first stage, the stress slowly increases as the strain increases because the 3D Gra-9 shrinks along the armchair direction and there is no graphene wall length change in the structure as shown in Figure 7. The stress is distributed uniformly as shown in **Figure 6**. With the increase of strain, the graphene wall in 3D Gra-9 along the zigzag direction are gradually straightened. When the strain reaches the value of 0.135, the

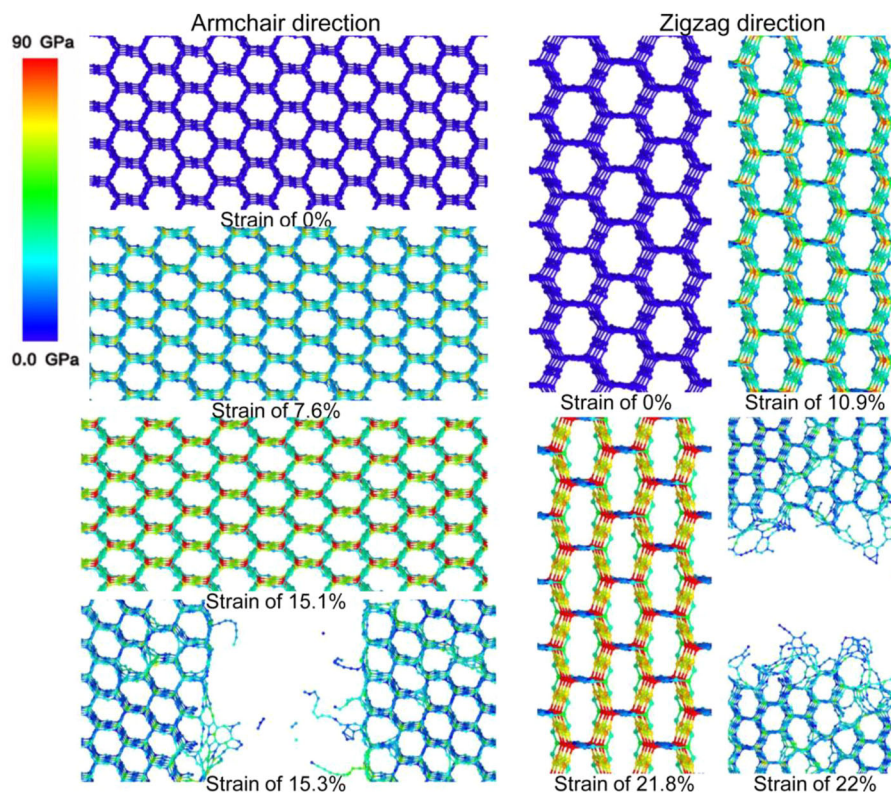


**Figure 5.** Atomic structural evolution of the 3D Gra-1 with thickness of 1.23 nm under tensile loading along armchair and zigzag direction at 300 K with strain rate of 0.001 ps<sup>-1</sup>. Atoms are colored based on the value of von Mises stress.

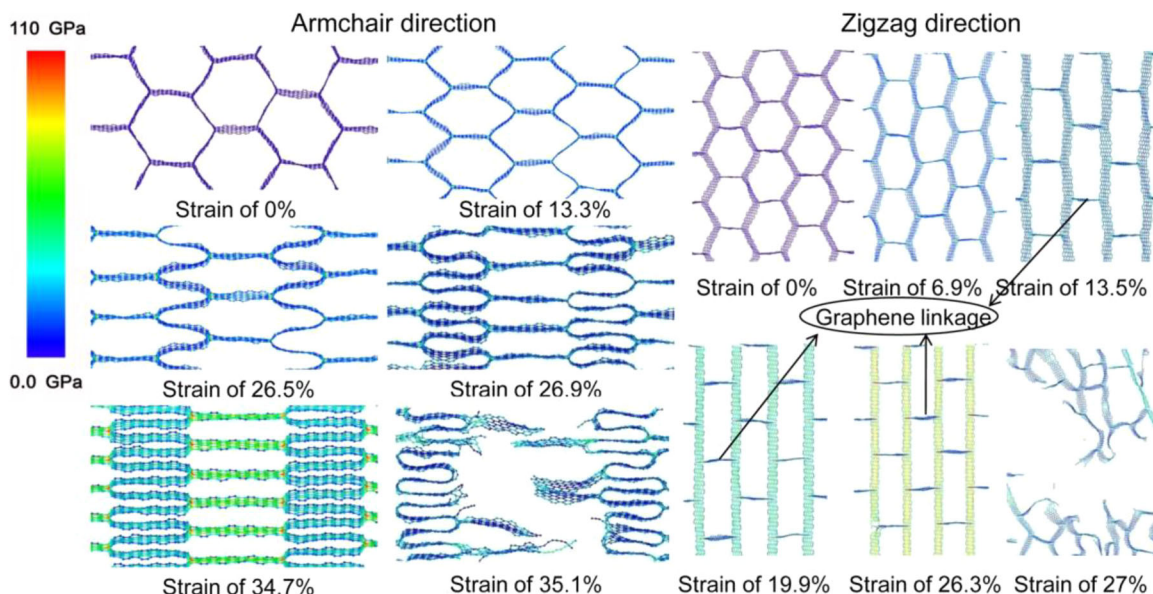


**Figure 6.** Atomic structural evolution of the 3D Gra-9 with thickness of 1.23 nm under tensile loading along armchair and zigzag direction at 300 K with strain rate of 0.001 ps<sup>-1</sup>. Atoms are colored based on the value of von Mises stress.

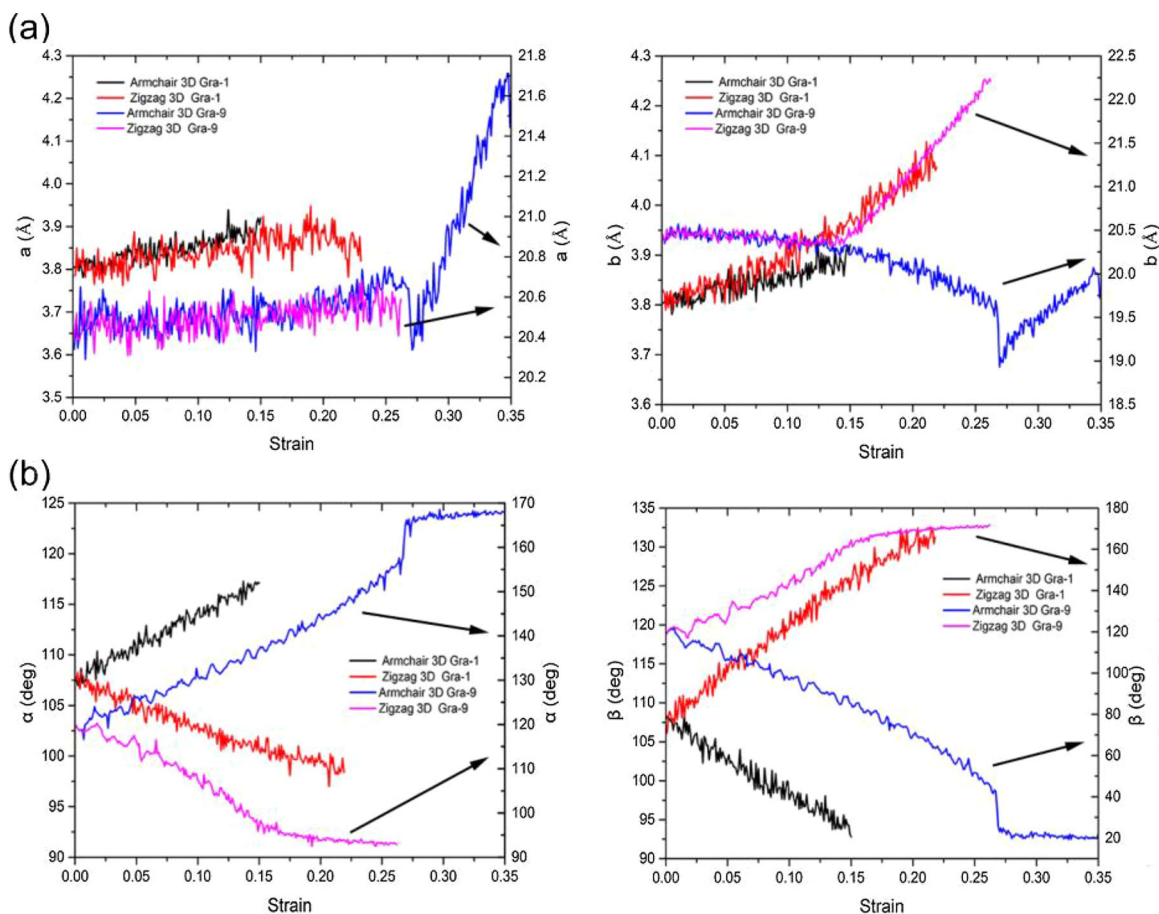


**Figure 7.** a) Variations of the graphene wall length and b) angle between two graphene walls with the strain during the tensile deformation along the armchair and zigzag directions.

hexagonal holes in 3D Gra-9 become rectangular. With the strain increasing further, in the second stage, we find that the deformations have been carried mainly through the elongation of the parallel graphenes. The graphene walls are stretched as shown in Figure 7. The stress begins to increase largely as the strain increase (see Figure 4). Finally, the graphenes break, as shown in Figure 6. For the tension along armchair direction, the first stage is similar to that along zigzag direction. The 3D Gra-9 undergoes a transverse shrinkage and the stress slowly increases as the strain. The stress is distributed uniformly as shown in Figure 6. The stress reaches the first peak value of 0.88 GPa with the strain of 0.265 which is about twice of 0.135 for zigzag direction. This is because 3D Gra-9 can hold larger structural deformation along armchair direction than that along zigzag direction as shown in Figures 6 and 7, which results in a larger fracture strain of tension along armchair direction than that along zigzag direction as the structure has similar elastic deformation along both armchair and zigzag direction before fracture as shown in Figure 4. Regarding to the sharp decrease of stress at the strain of 0.269 in the stress–strain curve for the tension along armchair direction, it is due to the transverse compressive buckling for which the graphene wall length and angle between two graphene walls are varied sharply as shown in Figure 7. However,

there is no sharp decrease of the stress in the stress–strain curve for the tension along zigzag direction because the graphene-like linkages (shown in Figure 6) prevent the structure from the transverse compressive buckling.

We also investigate the effects of the strain rate and temperature on the mechanical properties of 2D Graphene, 3D Gra-1 and -9 along both armchair and zigzag directions. The temperature varies from 100 to 1200 K and the strain rate varies from 0.001 to 0.02 ps<sup>-1</sup>. The variations of fracture stress and strain with the strain rate of 2D Graphene, 3D Gra-1 and -9 are shown in Figure 8a,b. It is seen that the fracture stress and strain along both armchair and zigzag directions are approximately linearly related to the strain rate. A slower strain rate results in a lower fracture stress and strain. When a lower strain rate is applied, the structure has more time to induce adequate local deformation, and hence the onset of plastic deformation is accelerated. The variations of fracture stress and strain with the temperature of 2D Graphene, 3D Gra-1 and -9 are shown in Figure 8c,d. The results clearly demonstrate that the fracture stress and strain along both armchair and zigzag directions decrease as the temperature increase. At higher temperature, the atoms vibrate about their

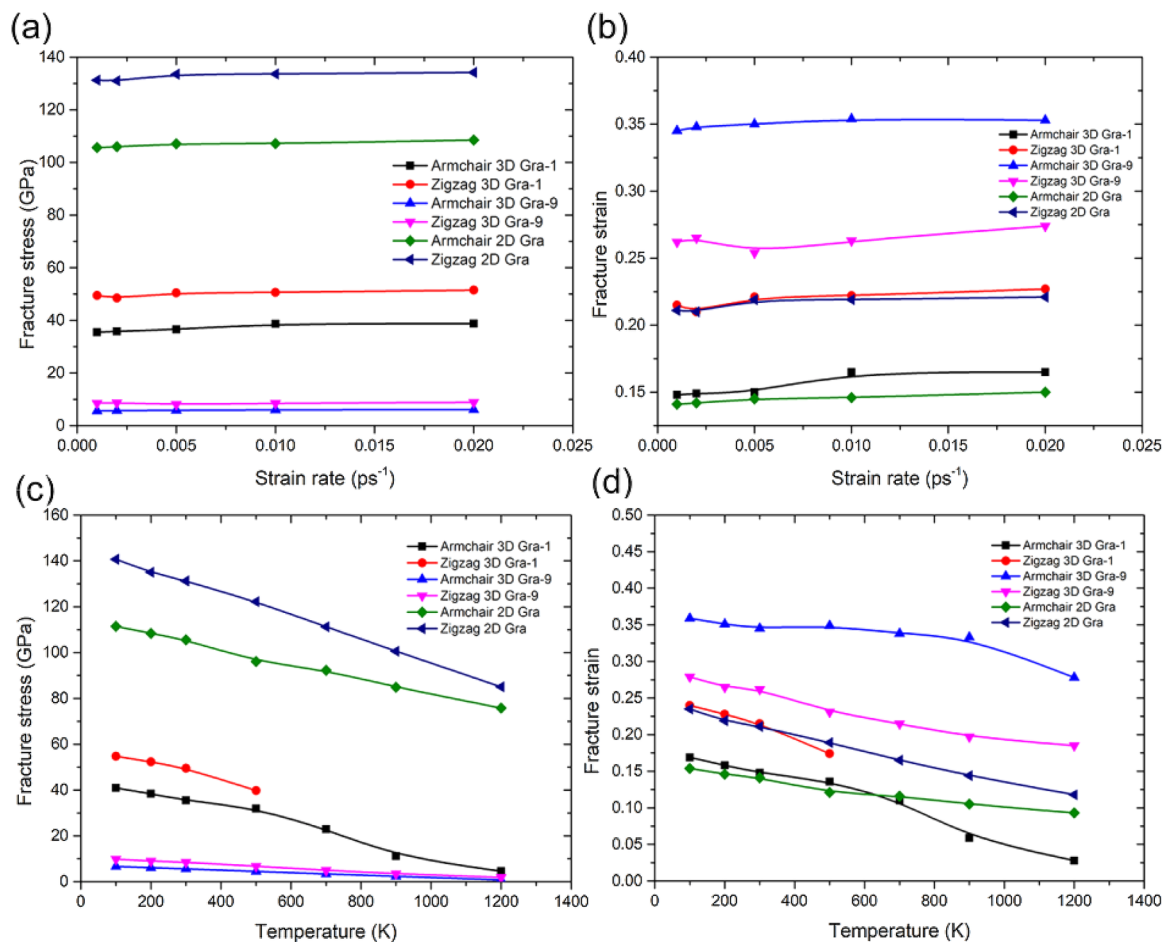


**Figure 8.** a) The variations of fracture stress b) and fracture strain with the strain rate, and c) fracture stress d) and fracture strain with the temperature for 2D Graphene, 3D Gra-1, and -9 along the armchair and zigzag directions.



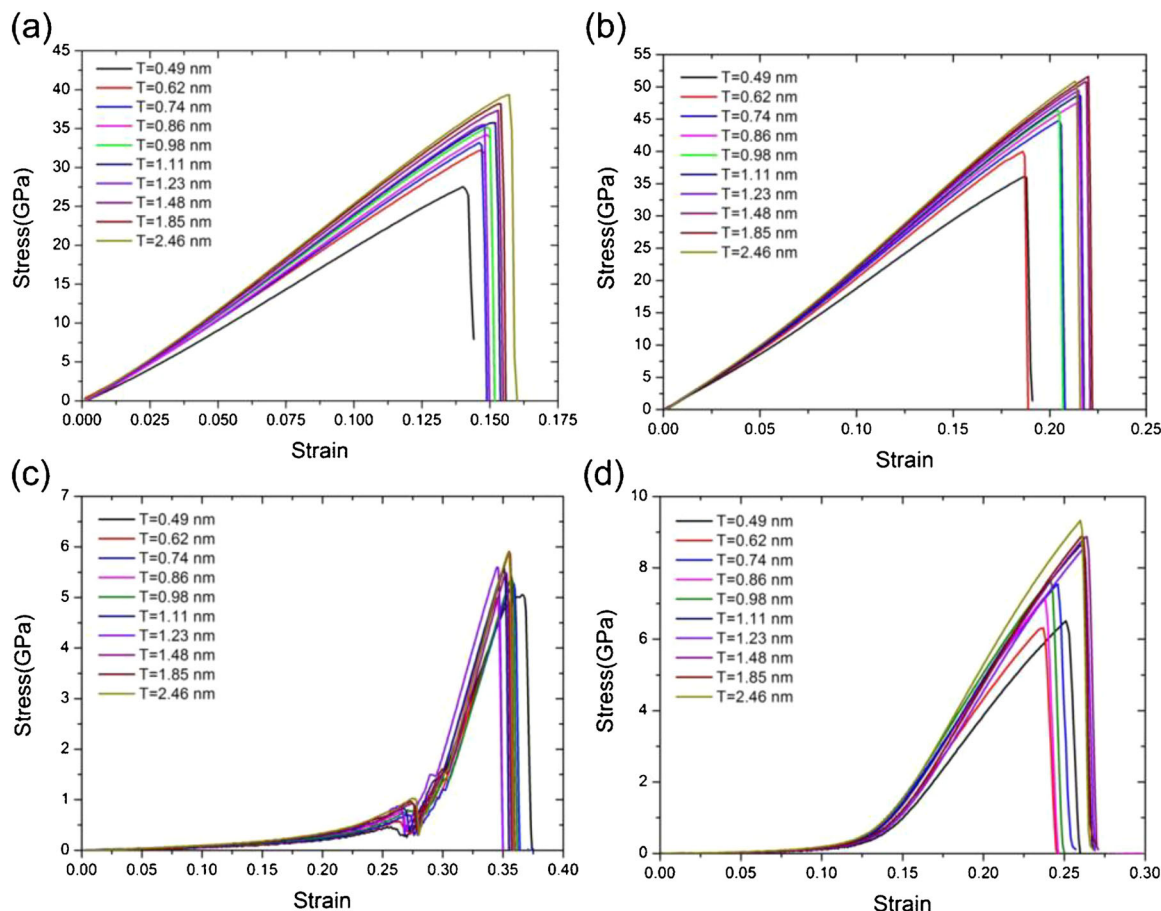


**Figure 9.** Stress–Strain curves of 3D graphene with different thickness: a) 3D Gra-1 along armchair direction and b) zigzag direction; c) 3D Gra-9 along armchair direction and d) zigzag direction simulated at 300 K with strain rate of 0.001 ps<sup>-1</sup>.

equilibrium position at much larger amplitude, a greater number of molecules gain sufficient energy to overcome the activation energy barrier, and hence deformation occurs. The present results demonstrate that the mechanical properties of

both 2D Graphene and 3D Graphene are sensitive to the strain rate and temperature conditions.

The thickness dependence of the mechanical properties of 3D graphene is also studied. The thickness varies from 0.36 to

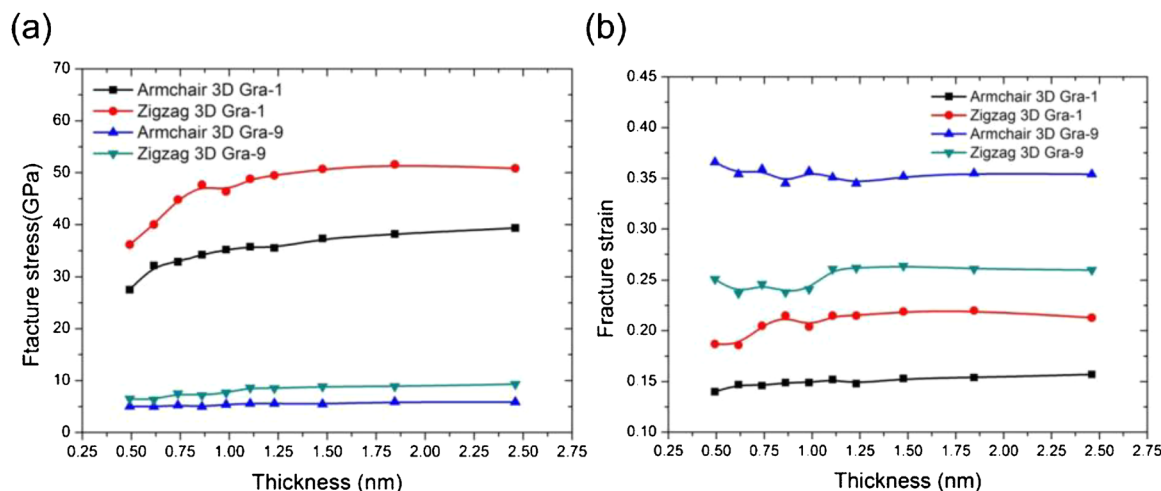


**Figure 10.** a) The variations of fracture stress and b) fracture strain with the thickness of 3D graphene along the armchair and zigzag directions at 300 K with strain rate of 0.001 ps<sup>-1</sup>.

2.05 nm. Two typical 3D graphene (3D Gra-1 and -9) are investigated. The stress–strain curves simulated at 300 K with strain rate of 0.001 ps<sup>-1</sup> are shown in **Figure 9**. It can be seen that both 3D Gra-1 and -9 show similar stress–strain curves for different thicknesses along both armchair and zigzag directions, which indicates that tensile deformation mechanisms are not dependent on the thicknesses of 3D graphene. The variations of fracture stress and strain with the thickness of 3D Gra-1 and -9 are shown in **Figure 10**. It can be found that the fracture stress for 3D Gra-9 along both armchair and zigzag directions is not dependent on the thickness. However, the fracture stress for 3D Gra-1 along both armchair and zigzag directions increases as the thickness increases, which indicates that the surface has considerable contribution at small thicknesses. In addition to the fracture stress, the fracture strain for both 3D Gra-1 and -9 is not dependent on the thickness.

## 4. Conclusions

In summary, in this paper, the mechanical properties and fracture mechanisms of 3D graphene under uniaxial tensile loading are investigated using MD simulations. It is found that the mechanical properties of 3D graphene is dependent on the in-plane cell size along both armchair and zigzag directions. By analyzing the atomic von Mises stress and structural evolution, the tensile deformation mechanism of 3D graphene is revealed. Compared to the 3D graphene with smaller in-plane cell size, the larger 3D graphene exhibits two typical deformation events, i.e., transverse structural shrinkage and axial elastic deformation. The fracture stress decreases monotonically with the increase of in-plane cell size and vary slightly for the larger size. The fracture stress of 3D graphene is much smaller than that of 2D graphene because of its porous structure. However, the fracture strain of 3D graphene increases as the in-plane cell size increases. In comparison with the fracture strain along zigzag direction, the fracture strain along armchair direction displays more obvious size dependence due to the larger transverse structural shrinkage ability along armchair direction than that along zigzag direction. The larger transverse structural shrinkage ability of 3D graphene with large in-plane cell results in a larger fracture strain than that of 2D graphene. In addition, the fracture stress and strain decrease as temperature increases, and the fracture stress and strain are approximately linearly dependent on the strain rate, which indicates that the temperature and strain rate exhibit significant effects on the mechanical response of both 2D and 3D graphene. However, fracture stress and strain are not largely dependent on the thickness of 3D graphene.

Our simulation results indicate that the 3D graphene with higher stretchability tunable by in-plane cell size could be promising multifunctional materials for many engineering applications.

## Acknowledgements

This research was supported by the NSF of China under Grants No. 11304059, the NSF of Heilongjiang Province of China under Grants No.

QC2015001, and the International Postdoctoral Exchange Fellowship Program No. 20140016.

## Conflict of Interest

The authors declare no conflict of interest.

## Keywords

3D graphene, fracture strain, molecular dynamics, size dependence, tensile deformation

Received: December 19, 2017

Revised: March 13, 2018

Published online: April 30, 2018

- [1] K. S. Novoselov, A. K. Geim, S. V. Morozov, D. Jiang, Y. Zhang, S. V. Dubonos, I. V. Grigorieva, A. A. Firsov, *Science* **2004**, 306, 666.
- [2] A. A. Balandin, S. Ghosh, W. Bao, I. Calizo, D. Teweldebrhan, F. Miao, C. N. Lau, *Nano Lett.* **2008**, 8, 90.
- [3] C. Lee, X. Wei, J. W. Kysar, J. Hone, *Science* **2008**, 321, 385.
- [4] B. Ouyang, F. Meng, J. Song, *2D Materials* **2014**, 1, 035007.
- [5] F. Meng, B. Ouyang, J. Song, *J. Phys. Chem. C* **2015**, 119, 3418.
- [6] Z. Jia, Z. Zuo, Y. Yi, H. Liu, D. Li, Y. Li, Y. Li, *Nano Energy* **2017**, 33, 343.
- [7] B. Mortazavi, M. Shahrokhi, T. Rabczuk, L. F. C. Pereira, *Carbon* **2017**, 123, 344.
- [8] Y. Xu, K. Sheng, C. Li, G. Shi, *ACS Nano* **2010**, 4, 4324.
- [9] Z. Niu, J. Chen, H. H. Hng, J. Ma, X. Chen, *Adv. Mater.* **2012**, 24, 4144.
- [10] F. Yavari, Z. Chen, A. V. Thomas, W. Ren, H. M. Cheng, N. Koratkar, *Sci. Rep.* **2011**, 1, 166.
- [11] Q. Chen, L. Zhang, G. Chen, *Anal. Chem.* **2011**, 84, 171.
- [12] N. V. Krainyukova, E. N. Zubarev, *Phys. Rev. Lett.* **2016**, 116, 055501.
- [13] H. R. Karfunkel, T. Dressler, *J. Am. Chem. Soc.* **1992**, 114, 2285.
- [14] Z. Pang, X. Gu, Y. Wei, R. Yang, M. S. Dresselhaus, *Nano Lett.* **2016**, 17, 179.
- [15] Z. Yang, G. Lan, B. Ouyang, L. C. Xu, R. Liu, X. Liu, J. Song, *Mater. Chem. Phys.* **2016**, 183, 6.
- [16] H. Eslami, L. Mohammadzadeh, N. Mehdipour, *J. Chem. Phys.* **2011**, 135, 064703.
- [17] H. Eslami, L. Mohammadzadeh, N. Mehdipour, *J. Chem. Phys.* **2012**, 136, 104901.
- [18] Z. Zhang, A. Kutana, Y. Yang, N. V. Krainyukova, E. S. Penev, B. I. Yakobson, *Carbon* **2017**, 113, 26.
- [19] F. Meng, C. Chen, D. Hu, J. Song, *J. Mech. Phys. Solid.* **2017**, 109, 241.
- [20] X. Gu, Z. Pang, Y. Wei, R. Yang, *Carbon* **2017**, 119, 278.
- [21] Y. Gao, Y. Chen, C. Zhong, Z. Zhang, Y. Xie, S. Zhang, *Nanoscale* **2016**, 8, 12863.
- [22] J. Song, B. Ouyang, *ACS Appl. Mater. Interfaces* **2013**, 5, 12968.
- [23] D. W. Brenner, O. A. Shenderova, J. A. Harrison, S. J. Stuart, B. Ni, S. B. Sinnott, *J. Phys. Cond. Matter* **2002**, 14, 783.
- [24] L. Lindsay, D. A. Broido, *Phys. Rev. B* **2010**, 81, 205441.
- [25] K. Min, N. R. Aluru, *Appl. Phys. Lett.* **2011**, 98, 013113.
- [26] Z. Yao, C. C. Zhu, M. Cheng, J. Liu, *Comp. Mat. Sci.* **2001**, 22, 180.
- [27] H. Zhao, K. Min, N. R. Aluru, *Nano Lett.* **2009**, 9, 3012.
- [28] S. Plimpton, *J. Comp. Phys.* **1995**, 117, 1.
- [29] W. G. Hoover, *Phys. Rev. A* **1985**, 31, 1695.
- [30] Q. X. Pei, Y. W. Zhang, V. B. Shenoy, *Nanotechnology* **2010**, 21, 115709.
- [31] Y. Jing, Y. Sun, H. Niu, J. Shen, *Phys. Status Solidi B* **2013**, 250, 1505.